Time-resolved coherent double Raman detection of nuclear spin transitions

Robert Klieber and Dieter Suter
Universität Dortmund, Fachbereich Physik, 44221 Dortmund, Germany
(Received 7 December 2005; published 8 March 2006)

Coherent Raman scattering can be used for detection of nuclear spin transitions in solids and atomic vapors if both nuclear spin states of the spin transition to be detected are connected to a single nuclear spin state of a different electronic state by allowed optical transitions. This is not the case in crystals with high symmetry. Here, we introduce the coherent double Raman experiment, where the difference between nuclear spin transitions in two different electronic states is observed. In contrast to the conventional Raman scattering experiment, this scheme is applicable also to systems with high symmetry, where the nuclear spin does not change during an optical transition.

DOI: 10.1103/PhysRevB.73.094408 PACS number(s): 76.70.Hb, 76.30.Kg, 32.10.Fn

I. INTRODUCTION

Optical detection of magnetic resonance transitions offers a number of advantages over conventional detection. Depending on the system under study, different techniques can detect magnetic resonance transitions by optical means. Here, we consider the coherent scattering of optical radiation by a coherent superposition of nuclear spin states. This approach, which is usually called coherent Raman scattering of Raman-heterodyne spectroscopy (RHS) has been developed by Wong and Mlynek[1,2] and applied to atomic vapors[3] as well as crystals of rare earth ions.[1,4,5]

For the general discussion of the coherent Raman process, we consider two electronic states g,e, which are split into two nuclear spin sublevels $\uparrow, \downarrow$ [see Fig. 1(a)]. If the system is prepared in a coherent superposition of the spin states $|g,\uparrow\rangle$ and $|g,\downarrow\rangle$ (which corresponds to a nuclear spin coherence), e.g., by a resonant radio frequency (rf) pulse [rf_1 in Fig. 1(a)], a laser field that couples the state $|g,\uparrow\rangle$ to $|e,\uparrow\rangle$ transfers this coherence from the ground state nuclear spin transition to the transition $|g,\downarrow\rangle \leftrightarrow |e,\uparrow\rangle$. If the optical transition matrix element for this transition is nonzero, this electronic coherence is the source of a Raman wave,[6,7] which can be detected by optical heterodyning. The resulting RHS signal is proportional to the product of the three matrix elements for the three transitions. In low-symmetry crystals all optical transition can be partly allowed and NMR spectra taken under such conditions allow one to probe electronic ground and electronically excited states.[2,4,8–11]

This is not the case in crystals with high symmetry: In this case, the nuclear spin part of the states are identical in the ground and excited states. Since the optical transition matrix does not contain the nuclear spin operator, only transitions between states with the same nuclear spin are allowed. In our example, the transitions $|g,\uparrow\rangle \leftrightarrow |e,\uparrow\rangle$, to which the laser couples, is optically allowed. However, the transition $|g,\downarrow\rangle \leftrightarrow |e,\uparrow\rangle$, to which the electronic coherence is transferred, is optically forbidden, i.e., the transition matrix element for this transition vanishes. As a result, the transferred coherence does not generate a Raman wave and cannot be detected under these conditions.

While the optical detection is not possible when the coherence is in the forbidden $|g,\downarrow\rangle \leftrightarrow |e,\uparrow\rangle$ transition, it is possible to observe it in the second optically allowed transition $|g,\downarrow\rangle \leftrightarrow |e,\downarrow\rangle$. This is achieved by exchanging the two nuclear spin sublevels of the electronically excited state, $|e,\downarrow\rangle$ and $|e,\uparrow\rangle$ by a resonant radio frequency pulse rf_2 in Fig. 1(b) applied to this transition. The overall result of the laser field and the rf fields is that the coherence is transferred from the nuclear spin transition to an allowed optical transition, where it again generates a Raman field. The frequency of this transition is given by the sum of the optical frequency and the difference between the two nuclear spin transitions. It thus carries information from the nuclear spin transitions in both electronic states.

In this paper, we introduce this experiment and implement it, using praseodymium-ions doped into an $YAlO_3$ as the test system. In Sec. III, we describe a time-resolved version of the conventional Raman heterodyne experiment, which is also the first step of the double Raman experiment that we discuss in Sec. IV. The paper concludes with a summary of the main results.

II. SCHEME

A. System and energy levels

The Pr^{3+} doped $YAlO_3$ crystal contains two inequivalent praseodymium sites. In this work, we consider the transition

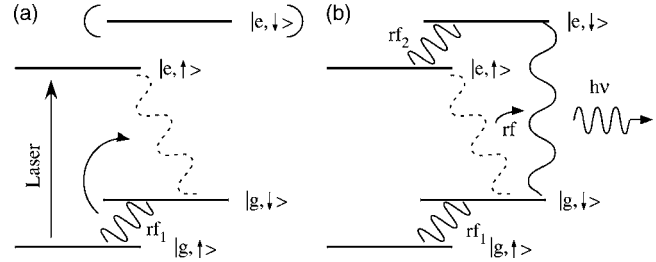

FIG. 1. Principle of coherent Raman scattering. (a) Nuclear coherence (coherent superposition between the states $|g,\downarrow\rangle$ and $|g,\uparrow\rangle$), excited by a radio frequency field (rf_1), can be detected with a laser field, if all involved transitions are allowed. The resulting optical polarization can be detected in a Raman heterodyne experiment. (b) If the Raman transition $|g,\downarrow\rangle \leftrightarrow |e,\uparrow\rangle$ is forbidden, no optical polarization is created. A second radio frequency field (rf_2), resonant with a nuclear spin transition in an electronically excited state, can transfer the optical coherence to the second optically allowed $|g,\downarrow\rangle \leftrightarrow |e,\downarrow\rangle$ transition.

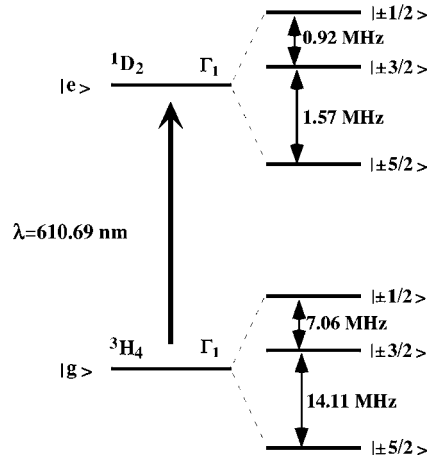

FIG. 2. Relevant part of the energy level scheme of $Pr^{3+}:YAlO_3$. The two electronic states consist of six nuclear spin substates each, which are pairwise degenerate in the absence of a static magnetic field.

between the lowest Stark component Γ_1 of the electronic state $^3H_4$ and the electronically excited $^1D_2$ state, which is centered at a wavelength of 610.69 nm. Since the Pr nuclear spin is $I=5/2$, the electronic states split into six hyperfine states. All 36 optical transitions between the $^3H_4$ and the $^1D_2$ sublevels are weakly allowed due to the low site symmetry C_{1h}.[12] A narrow homogeneous optical linewidth of approximately 10 kHz at low temperatures results from a long lifetime of the excited state ($T_1=180\ \mu$s[13,14]). In the presence of an external magnetic field the optical transition has a dephasing time of $T_2=78\ \mu$s.[13,15]

The nuclear spin Hamiltonian for the quadrupole- and the Zeeman-interaction can be described in the principal axis system of the Pr^{3+} quadrupole tensor by

$$H = H_Q + H_Z,$$

where

$$H_Q = D\left[I_z^2 - \frac{1}{3}I(I+1)\right] + E(I_x^2 - I_y^2),$$

$$H_Z = -B_0\hbar(\gamma_x I_x \sin\theta\cos\phi + \gamma_y I_y \sin\theta\sin\phi + \gamma_z I_z \cos\theta).$$

The polar angles θ and ϕ describe the orientation of the external magnetic field B_0 in the principal axis system of the nuclear spin. The γ_i are the principal elements of the gyromagnetic tensor.[5,16] The $m_I=\pm 5/2$ are the energetically lowest states, since the quadrupole coupling constants D and E are negative.[9,10] In crystals with high symmetry, the direction of the principal axes of quadrupole and Zeeman tensors are aligned with the symmetry axes. As a result, the nuclear spin state does not change during an optical transition ($\Delta m_I=0$).

Figure 2 shows the relevant part of the energy-level scheme of the $^3H_4$ and $^1D_2$ states. For vanishing external static magnetic fields each electronic state consists of three doubly degenerate hyperfine states; the resulting splittings are of the order 7.1, 14.1, and 21.2 MHz in the $^3H_4$- and 0.9, 1.6, and 2.5 MHz in $^1D_2$-state.[17]

TABLE I. Nuclear spin transition frequencies of the $m_I=\pm 1/2\leftrightarrow\pm 3/2$ transitions in the $^3H_4$- and $^1D_2$-state for a static B-field of 7.2 mT.

State	Site	Frequency [MHz]			
$^3H_4$	$1g$	6.35	6.94	7.22	7.79
	$2g$	5.83	6.60	7.59	8.26
$^1D_2$	$1e$	0.64	0.81	1.08	1.25
	$2e$	0.65	0.78	1.11	1.24

If the degeneracy is lifted by a static magnetic field, each optical transition splits into four, which are (partly) allowed. The two crystallographically inequivalent sites result into eight observable resonance lines centered at each of the frequencies indicated in Fig. 2.[4,5,18] A resonant radio frequency magnetic field can induce transitions between all nuclear spin states.[12,19] Table I lists the resonance frequencies for the $m_I=\pm 1/2\leftrightarrow\pm 3/2$ nuclear spin transitions in the $^3H_4$ electronic ground state and the $^1D_2$ electronically excited state for a magnetic field of 7.2 mT oriented at an angle of 5.7° from the b- and perpendicular to the crystal c axis.

B. Pulsed excitation

In the experiments, we use pulsed excitation of the nuclear spin transitions as well as of the optical transitions. To describe the time evolution of the system during these pulse sequences, we use a density operator formalism and the virtual spin-1/2 formalism of Wokaun and Ernst.[20] The Hamiltonian for a general radio frequency pulse applied close to resonance with the transition $i\leftrightarrow j$, is

$$\hat{H} = -\hbar(\Delta\omega_{ij}\hat{S}_z^{ij} + \omega_x\hat{S}_x^{ij}),$$

where ω_x is the nutation frequency and proportional to the amplitude of the applied rf or laser field. $\Delta\omega_{ij}$ describes the detuning of the transition $i\leftrightarrow j$ from the frequency of the field, and S_α^{ij} are the single transition operators.[20]

A resonant x-pulse rotates a spin state around the x-axis in the Bloch sphere. If the field is applied off resonance (i.e., $\Delta\omega_{ij}\neq 0$), the rotation axis is tilted away from the z-axis by

$$\theta = \arctan\left(\frac{\omega_x}{\Delta\omega_{ij}}\right).$$

The magnitude of the rotation frequency around the tilted axis is given by the effective strength $\omega_{\mathrm{eff}_{ij}}$ of the applied rf or laser field. The rotation angle for an off-resonant pulse is

$$\beta = \omega_{\mathrm{eff}_{ij}}\cdot\tau = \sqrt{\omega_x^2 + \Delta\omega_{ij}^2}\cdot\tau,$$

where τ denotes the pulse duration. Therefore, the rotation operator for an x-pulse with off-resonance effects is given by

$$\hat{R}^{ij}(\beta) = e^{-i\tau\hat{H}} = \hat{R}_y^{ij}(\theta)\hat{R}_z^{ij}(\beta)\hat{R}_y^{ij}(-\theta).$$

A resonant $\pi/2$-pulse ($\beta=\pi/2, \theta=\pi/2$) creates a maximal coherent superposition between the two states that resonant field couples. A π-pulse can be used to interchange

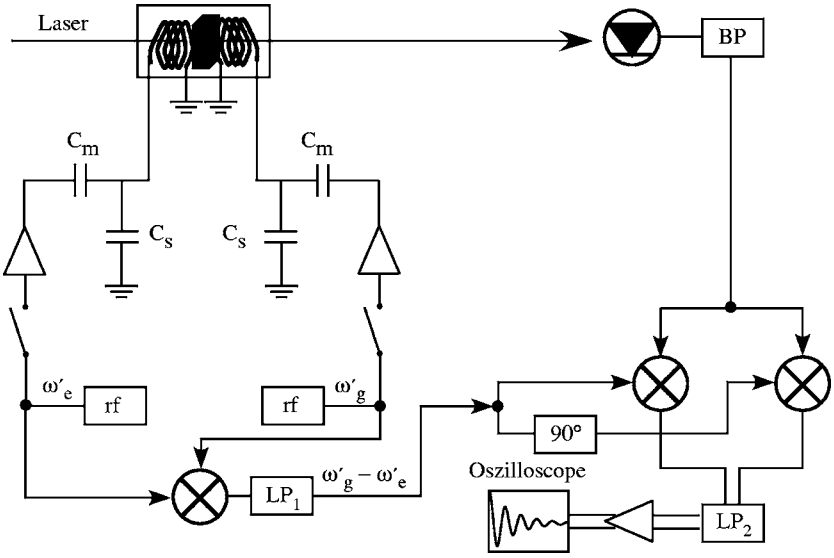

FIG. 3. Experimental setup: BP is a band-pass filter (3–10 MHz), LP_1 is a low-pass filter (7.5 MHz), rf are the radio frequency generators producing the radio frequencies ω'_g and ω'_e, and 90° is a $\pi/2$ phase delay.

coherence completely between different electronic or nuclear transitions.

C. Experimental

For these initial studies, we chose a system in which conventional Raman heterodyne detection works. A well characterized sample is $Pr:YAlO_3$.[15,16,21] We used a crystal with a 0.75% Pr concentration. Optical excitation and detection used the 610.69 nm transition between the $^3H_4$ ground and the $^1D_2$ excited state.

Figure 3 shows the experimental setup. An actively stabilized ring dye laser (Coherent 899-21) generated a linearly polarized laser beam, which was focused to a spot size of 100 μm in the sample, propagating along the crystal c-axis.

The sample was cooled to 3 K in a helium flow cryostat and mounted between a pair of small rf coils with one resonance circuit for each coil. The resonance frequency of the first circuit was $\omega'_g = 6.58$ MHz, i.e., in the region of the ground state transitions, the frequency of the second circuit was $\omega'_e = 1.12$ MHz, resonant with the excited state transitions.

III. PULSED RAMAN HETERODYNE NMR

A. Theoretical description

For the excitation and detection of ground state nuclear spin coherence, we consider two levels in the electronic ground state ($|g,\downarrow\rangle$ and $|g,\uparrow\rangle$), which are connected by optical transitions to the electronically excited state $|e,\uparrow\rangle$. The laser frequency is resonant with the transition from $|g,\uparrow\rangle$ to $|e,\uparrow\rangle$. Figure 4 illustrates the timing of the laser and the radio frequency pulses for this experiment.

We first apply a π laser pulse to empty the $|g,\uparrow\rangle$ state and thereby create a large nuclear spin polarization in the electronic ground state. After the laser pulse, the traceless part of the ground state density operator is proportional to

$$\hat{\rho}_0 = \hat{S}_z^{g\downarrow,g\uparrow}.$$

The density operator component proportional to the unity operator $\hat{1}^{g\downarrow,g\uparrow}$ can be neglected, since it is time-independent and does not contribute to the signal.

A radio frequency (rf) pulse that is resonant with the ground state nuclear spin transition $|g,\downarrow\rangle \leftrightarrow |g,\uparrow\rangle$ converts the population difference into coherence (a superposition of the states $|g,\downarrow\rangle$ and $|g,\uparrow\rangle$), as indicated by inset ① in Fig. 4. After a β_1-radio frequency pulse, the coherence between the nuclear spin levels becomes

$$\hat{\rho}_1 = \hat{R}^{g\downarrow,g\uparrow}(\beta_1)\rho_0\hat{R}^{g\downarrow,g\uparrow}(-\beta_1) = A\hat{S}_x^{g\downarrow,g\uparrow} + B\hat{S}_y^{g\downarrow,g\uparrow}, \quad (1)$$

where

$$A = (1-\cos\beta_1)\sin\theta_1\cos\theta_1, \quad B = \sin\beta_1 \sin\theta_1$$

After the pulse, the nuclear spin coherence is allowed to evolve freely, and its evolution is detected via coherent Raman scattering[7] by applying a weak laser frequency field. The laser field transfers the coherence from the nuclear spin transition to the optical $|g,\downarrow\rangle \leftrightarrow |e,\uparrow\rangle$ transition (instance ② in Fig. 4). If this transition is allowed (which is the case in the system chosen for this study), it gives rise to a coherent

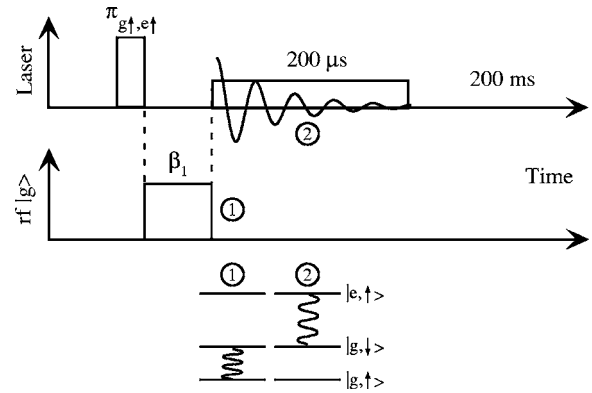

FIG. 4. Timing of the laser and radio frequency fields. The top trace shows the laser pulses, the bottom trace the radio frequency pulse. The second laser pulse is used for detection of the nuclear spin coherence by coherent Raman scattering. The pictures at the bottom show the energy level scheme assumed for the calculation and the existing coherences for two instances during the pulse sequence.

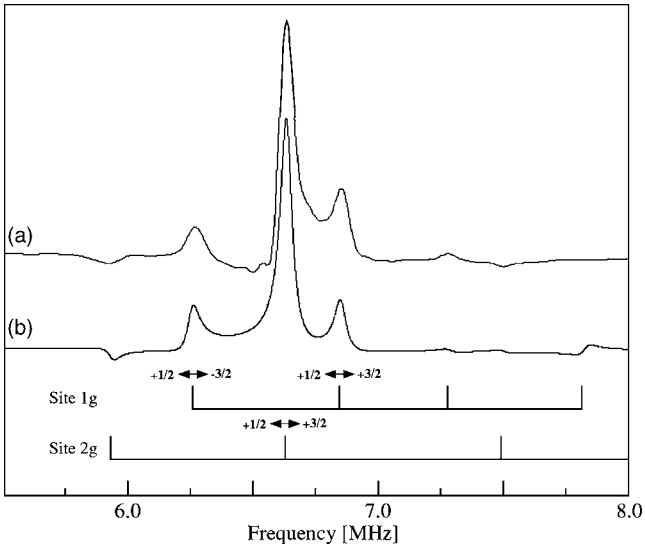

FIG. 5. (a) Experimental Raman heterodyne spectrum for the $^3H_4$ $m_I=\pm 1/2 \leftrightarrow \pm 3/2$ transitions of Pr^{3+}:$YAlO_3$ at 3 K. The external magnetic field was 7.2 mT. (b) Theoretical spectrum obtained from Eq. (2). The vertical lines in the lower part of the figure denote seven of the eight possible resonance line positions.

Raman field, which is then detected by optical heterodyne detection. In the experiment, this was achieved with a 200 MHz photodetector. The optical beat signal, which oscillates at the frequency ω_g, is phase-sensitively detected using the ground-state radio frequency ω_g' as the reference. The resulting signal is

$$s(t) \sim (A - iB)e^{-i\Delta\omega_g t}e^{-t/T_{2m}^{\star}} \qquad (2)$$

Here, the precession frequency $\Delta\omega_g$ is given by the difference between the Zeeman frequency of the ground state nuclear spin ω_g and the applied ground-state radio frequency ω_g'. The free induction decay (FID) signal amplitude decays with the transversal magnetic relaxation time $T_{2m}^{\star}$.

B. Ground state

Raman heterodyne signals with pulsed excitation were measured for the $m_I=\pm 1/2 \leftrightarrow \pm 3/2$ transitions in the $^3H_4$ and $^1D_2$ state, using the pulse sequence of Fig. 4. The radio frequency field was applied along the crystal c-axis with an amplitude of approximately 2.8 mT for the electronic ground state and 6.5 mT for the electronically excited state. The intensity of the pump- and detection-pulses was 1.5 MW/m^2 and 16 kW/m^2, respectively. The π-pulse-length for an optical pump-pulse was determined in a standard photon echo experiment and found to be 500 ns at 3 K. The laser frequency was swept linearly over 2 GHz within 25 s during the whole experiment to bring it into resonance with different ions in thermal equilibrium for subsequent shots. A good signal-to-noise ratio was achieved with some 2000 accumulated FID's.

Figure 5 shows the resulting Raman heterodyne spectrum obtained for the $^3H_4$-state. For this experiment, the radio frequency was set to 6.58 MHz, within the range of the $\pm 1/2 \leftrightarrow \pm 3/2$ transitions of the electronic ground state. With the available rf field strength (Rabi frequency $\approx$100 kHz), it was not possible to simultaneously excite all eight transitions, which are spread over a range of more than 2 MHz in the field of 7.2 mT. The vertical lines at the bottom of Fig. 5 show the expected positions of the resonance lines (which were verified by conventional cw Raman heterodyne spectroscopy), and Fig. 5(b) shows the theoretical spectrum calculated with the parameters given above. The different amplitudes in the spectrum result from off-resonance effects and from different transition matrix elements. Table II lists the relevant matrix elements, which were calculated for the $^3H_4$-state for a static B-field of 7.2 mT with the orientation summarized in Table III. The width of the resonance lines is determined by the transverse spin relaxation time $T_{2m}^{\star}(\approx 35\ \mu s)$.

TABLE II. Magnetic dipole matrix elements for the $m_I=\pm 1/2 \leftrightarrow \pm 3/2$ transitions in the $^3H_4$-state for a static B-field of 7.2 mT.

Site	$1g$		$2g$	
g/g	$\|+3/2\rangle$	$\|-3/2\rangle$	$\|+3/2\rangle$	$\|-3/2\rangle$
$\|+1/2\rangle$	1.26	0.743	1.372	0.442
$\|-1/2\rangle$	0.658	1.213	0.371	−1.353

C. Excited state

Equation (2) applies equally well to nuclear coherences excited in the excited state $^1D_2$. In this case the radio frequency field has to be resonant with a nuclear transition in the electronically exited state. We chose again the $\pm 1/2 \leftrightarrow \pm 3/2$ transitions, whose resonance frequencies in the electronically excited state are close to 1 MHz.

Figure 6 shows a comparison between the calculated and the experimental Raman spectrum for the $^1D_2$-state. The theoretical spectrum was calculated using Eq. (2) and assuming a nuclear spin relaxation time $T_{2m}^{\star}$ of 85 μs and a Rabi frequency of $\omega_x'=110$ kHz. The individual transition matrix elements are summarized in Table IV.

Remaining deviation between the theoretical and the experimental spectra result from the simplifications we made. As an example we did not take the experimental low pass filter (LP_2:400 kHz) into account, which influences the phase and the amplitude of the resonance-lines in the experimental spectra.

TABLE III. Orientation of the magnetic field in the principal axis systems of both sites and both electronic states.

State	Site	ϕ [°]	θ [°]
$^3H_4$	$1g$	90	68.4
	$2g$	90	44.4
$^1D_2$	$1e$	90	69.6
	$2e$	90	86.4

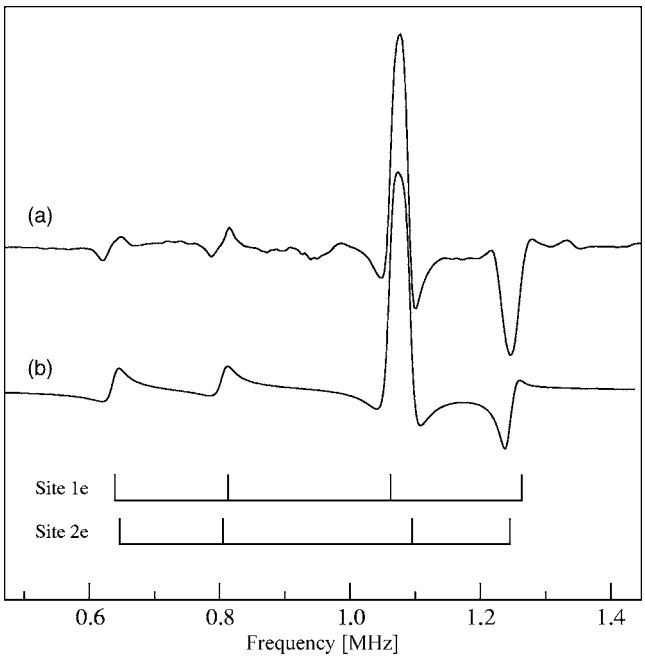

FIG. 6. (a) Experimental Raman heterodyne spectrum for the $D_2{}^1$ $m_I=\pm 1/2 \leftrightarrow \pm 3/2$ transitions of Pr^{3+}:$YAlO_3$ at 3 K. The external magnetic field was 7.2 mT. (b) Spectrum calculated from Eq. (2). The vertical lines in the lower part of the figure denote the eight resonance line positions.

IV. DOUBLE RAMAN SPECTRA

A. Procedure

The above experiments use the fact that the coherent Raman process transfers the nuclear spin coherence into an optical transition with a nonvanishing transition matrix element. In systems where this matrix element vanishes, the resulting coherence does not give rise to a Raman field and cannot be detected. This problem can only be avoided if the coherence is transferred again, into an optically allowed transition, where it can be detected by optical heterodyning.

For this experiment we consider two nuclear spin states in the electronic ground state ($|g,\downarrow\uparrow\rangle$) and two in the excited state ($|e,\downarrow\uparrow\rangle$), which are connected by optical transitions. Figure 7 illustrates the timing of the external fields (laser, rf) that drive the system and transfer the coherence between the different transitions. For optical pulses we consider ideal pulses, but for the rf-pulses, we take off-resonance effects into account.

The experiment starts with an optical π pulse and a radio frequency $\pi/2$ pulse applied to the ground state nuclear spin

TABLE IV. Magnetic dipole transition matrix elements for the $m_I=\pm 1/2 \leftrightarrow \pm 3/2$ transitions in the $^1D_2$-state for a static B-field of 7.2 mT.

Site	$1e$		$2e$	
e/e	$\|+3/2\rangle$	$\|-3/2\rangle$	$\|+3/2\rangle$	$\|-3/2\rangle$
$\|+1/2\rangle$	−1.597	−0.570	−1.705	−0.122
$\|-1/2\rangle$	0.398	−1.301	−0.085	1.340

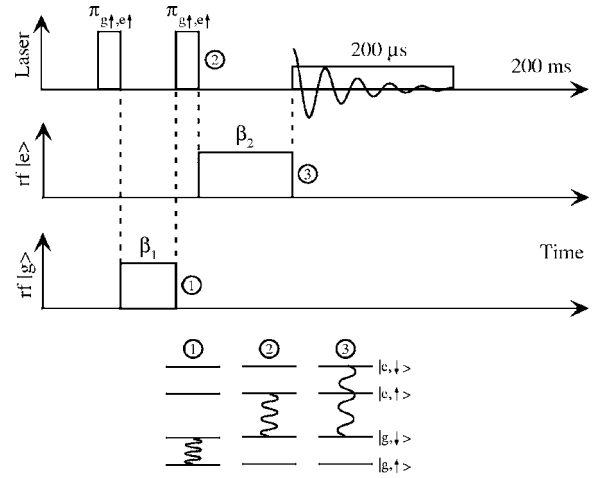

FIG. 7. Timing of the laser and the radio frequency pulses. The top trace shows the laser pulses, the center trace the radio frequency pulse that is resonant with the excited state $m_I=\pm 1/2 \leftrightarrow \pm 3/2$ transitions, and the bottom trace the pulse that is resonant with the corresponding ground state transitions. The detection uses a weak laser pulse for Raman heterodyne detection of the ground state nuclear spin coherence. The diagrams at the bottom show the energy level scheme used for the calculation and the coherences for three instances during the pulse sequence.

transition, as in the case discussed above. The resulting state is, therefore, described by Eq. (1). Instead of measuring the resulting spin coherence by a Raman heterodyne process, we now transfer it into an optical coherence by applying a π_x-laser-pulse to the $|g,\uparrow\rangle \leftrightarrow |e,\uparrow\rangle$ transition. The resulting state is

$$\hat{\rho}_2 = \hat{R}^{g\uparrow,e\uparrow}(\pi)\hat{\rho}_1\hat{R}^{g\uparrow,e\uparrow}(-\pi) = -A\hat{S}_y^{g\downarrow,e\uparrow} + B\hat{S}_x^{g\downarrow,e\uparrow},$$

i.e., a coherence in the $|g,\downarrow\rangle \leftrightarrow |e,\uparrow\rangle$ transition. Note that the nuclear spin state differs for the two states.

This coherence can be transferred into a different optical transition by applying an rf pulse to a suitable nuclear spin transition in the electronically excited state. For a β_2-pulse, we obtain

$$\hat{\rho}_3 = \hat{R}^{e\downarrow,e\uparrow}(\beta_2)\hat{\rho}_2\hat{R}^{e\downarrow,e\uparrow}(-\beta_2) = C(A\hat{S}_x^{g\downarrow,e\downarrow} + B\hat{S}_y^{g\downarrow,e\downarrow}), \quad (3)$$

where

$$C = -2\sin\frac{\theta_2}{2}\cos\frac{\theta_2}{2}\sin\frac{\beta_2}{2}.$$

Since the coherence is now between states with identical nuclear spin part, it is optically allowed even in systems where the crystal symmetry determines the spin state. It can be detected by optical heterodyning, i.e., by superimposing a weak laser beam. The resulting beat signal was again demodulated, using now the difference between the ground- and the excited-state radio frequencies as the reference. The demodulated signal is then

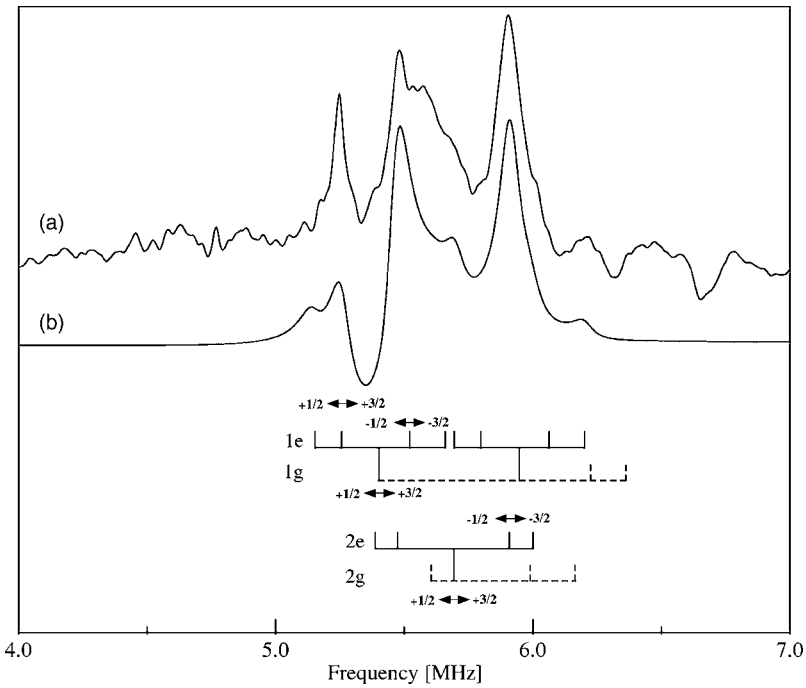

FIG. 8. (a) Experimental double Raman spectrum of $Pr^{3+}:YAlO_3$ at 3 K. The external magnetic field is 7.2 mT. (b) Spectrum calculated from Eq. (4). The vertical lines in the lower part of the figure denote the twelve main resonance line positions.

$$s(t) \sim C(B + iA)e^{-t/T_2^{\star}} e^{-i\Delta\omega_{ge}t}. \quad (4)$$

The beat signal between Raman and laser field equals the difference between the Zeeman frequencies of the ground and excited state nuclear spin transitions ($\omega_g - \omega_e$). This signal is then demodulated with the difference of the two radio frequencies used for the excitation, $\omega_g' - \omega_e'$. The resulting frequency is given thus $\Delta\omega_{ge} = \omega_g - \omega_e - (\omega_g' - \omega_e')$. The FID signal amplitude decays with the optical transverse relaxation time $T_2^{\star}$.

B. Experimental results

The Raman field and the transmitted part of the laser field were measured with the experimental setup of Fig. 3. After the signal was amplified and demodulated with the difference frequency of the two applied radio frequency fields, it was lowpass-filtered (LP_2: 1.5 MHz) and measured with a digital oscilloscope. All other experimental parameters are described in Sec. III.

Figure 8 shows the calculated spectrum obtained from Eq. (4) and the experimental double Raman spectrum.

In the system that we used for these experiments, the Raman coherences excited by the individual rf pulses and the laser pulses also give rise to an observable optical heterodyne signal (see Sec. III). However, these signal contributions depend only on the phase of the rf pulse that excited them. Since the signal shown here is demodulated with the difference of both rf signals, only signal components that vary with the phase of both rf fields are obtained after the averaging process. In the experiment, we averaged over 2000 FID's, resulting in a high suppression ratio for single-rf signal contributions. As an additional check, we also performed the experiment with either of the two rf excitation pulses switched off and found no observable signal.

The signals observed in these spectrum occur at differences between the nuclear spin transition frequencies of the two electronic states. Since each site has four transitions in each electronic state, we expect a total of 32 resonance lines in this spectrum. However, the calculation shows that only 12 of them are significantly different from zero under our experimental conditions. These line positions are indicated by the vertical lines in the lower part of the spectrum in Fig. 8.

Figure 9 compares the Raman heterodyne spectra obtained with a single rf-field to that obtained with the double-rf-field. The one-rf spectrum of the ground state and the double-rf spectrum overlap between 5.8 and 6.5 MHz (Fig. 8: Frequency positions >0.8 MHz). Peaks at frequency-positions of ground state transitions can be found in the double-rf spectrum, indicating that some coherence from the double-rf transition was transferred back to the one-rf transition during the last rf pulse (the pulse is not an ideal π-pulse for all nuclear spin transitions). The transferred coherences carry phase information of the radio frequency field applied in the excited state and therefore add to the signal amplitude in the double-rf spectrum at the positions of the ground state spectrum.

This modification of the Raman heterodyne technique allows us to measure Raman heterodyne signals for samples with forbidden optical transitions, which are not detectable in a standard Raman heterodyne setup. In this experiment the rf pulses have to be short in relation to the optical transversal dephasing time. The sensitivity is reduced compared to the conventional experiment, since every coherence transfer involves losses due to experimental imperfections and additional signal channels (i.e., larger number of resonance lines). The faster decay of the signal in the optical transition, compared to the magnetic transition also reduces signal amplitude and resolution.

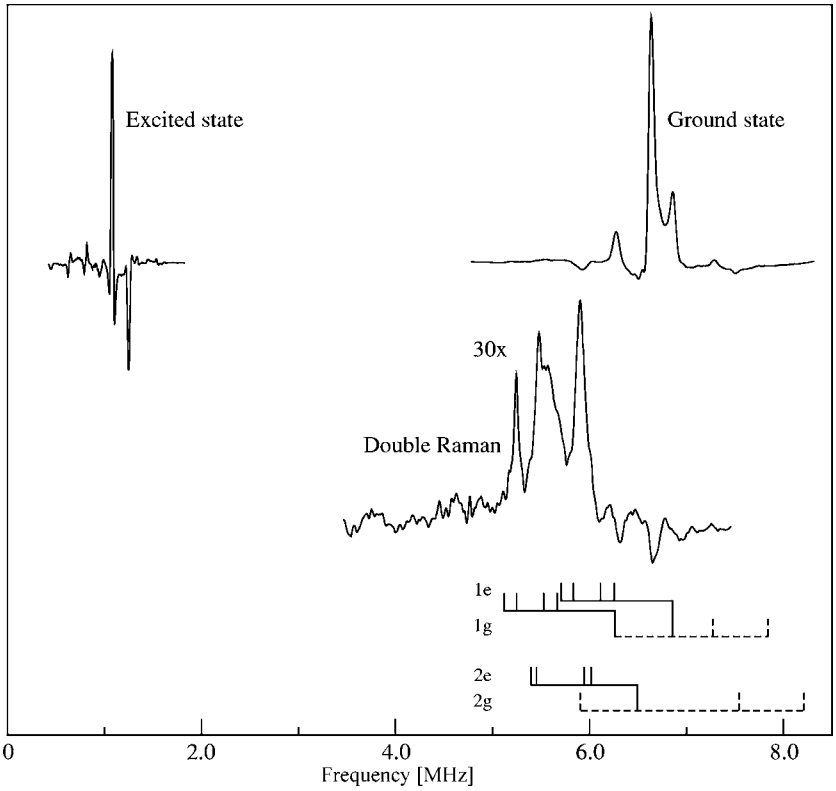

FIG. 9. Absorptive part of the two experimental one-rf and the double-rf excited Raman heterodyne signals in $Pr^{3+}:YAlO_3$ at 3 K. The external magnetic field is 7.2 mT.

V. CONCLUSION

In this article we have demonstrated a time-resolved coherent double Raman experiment that allows one to optically detect nuclear spin transitions. The resulting signals occur at the difference between the ground- and excited-state transition frequencies. This technique should be applicable to other systems with higher crystal symmetry as well, where nuclear spin coherences can be excited by radio frequency fields, but are not detectable in a standard Raman heterodyne experiment.

ACKNOWLEDGMENT

This work was supported by the DFG through Grant No. Su 192/4-3.

[1] J. Mlynek, N. C. Wong, R. G. DeVoe, E. S. Kintzer, and R. G. Brewer, Phys. Rev. Lett. **50**, 993 (1983).
[2] N. C. Wong, E. S. Kintzer, J. Mlynek, R. G. DeVoe, and R. G. Brewer, Phys. Rev. B **28**, 4993 (1983).
[3] J. Mlynek, C. Tamm, E. Buhr, and N. C. Wong, Phys. Rev. Lett. **53**, 1814 (1984).
[4] M. Mitsunaga, E. S. Kintzer, and R. G. Brewer, Phys. Rev. Lett. **52**, 1484 (1984).
[5] M. Mitsunaga, E. S. Kintzer, and R. G. Brewer, Phys. Rev. B **31**, 6947 (1985).
[6] E. Garmire, F. Pandarese, and C. H. Townes, Phys. Rev. Lett. **11**, 160 (1963).
[7] J. A. Giordmaine and W. Kaiser, Phys. Rev. **144**, 676 (1966).
[8] L. E. Erickson, Phys. Rev. B **32**, 1 (1985).
[9] T. Blasberg and D. Suter, Phys. Rev. B **48**, 9524 (1993).
[10] R. Klieber, A. Michalowski, R. Neuhaus, and D. Suter, Phys. Rev. B **67**, 184103 (2003).
[11] R. Klieber and D. Suter, Phys. Rev. B **71**, 224418 (2005).
[12] S. Hüfner, *Optical Spectra of Transparent Rare Earth Compounds* (Academic Press, New York, 1978).
[13] M. Mitsunaga, N. Uesugi, and K. Sugiyama, Opt. Lett. **18**, 1256 (1993).
[14] R. M. MacFarlane and R. M. Shelby, in *Spectroscopy of Solids Containing Rare Earth Ions*, edited by A. Kaplyanskii and R. M. MacFarlane (North-Holland, Amsterdam, 1987).
[15] R. M. Macfarlane, R. M. Shelby, and R. L. Shoemaker, Phys. Rev. Lett. **43**, 1726 (1979).
[16] L. E. Erickson, Phys. Rev. B **19**, 4412 (1979).
[17] L. E. Erickson, Phys. Rev. B **16**, 4731 (1977).
[18] L. E. Erickson, Phys. Rev. B **42**, 3789 (1990).
[19] M. H. Cohen, Phys. Rev. **96**, 1278 (1954).
[20] A. Wokaun and R. R. Ernst, J. Chem. Phys. **67**, 1752 (1977).
[21] R. M. MacFarlane, J. Lumin. **100**, 1 (2002).